Origin of the Energy Barrier to Chemical Reactions of O_2 on Al(111): Evidence for Charge Transfer, Not Spin Selection

Florian Libisch,[1] Chen Huang,[2] Peilin Liao,[1] Michele Pavone,[1,*] and Emily A. Carter[1,†]

[1]*Departments of Mechanical and Aerospace Engineering and Chemistry, Program in Applied and
Computational Mathematics, and Andlinger Center for Energy and the Environment,
Princeton University, Princeton, New Jersey 08544, USA*
[2]*Theoretical Division, Los Alamos National Laboratory, New Mexico 87544, USA*
(Received 10 January 2012; published 8 November 2012)

Dissociative adsorption of molecular oxygen on the Al(111) surface exhibits mechanistic complexity that remains surprisingly poorly understood in terms of the underlying physics. Experiments clearly indicate substantial energy barriers and a mysteriously large number of adsorbed single oxygen atoms instead of pairs. Conventional first principles quantum mechanics (density functional theory) predicts no energy barrier at all; instead, spin selection rules have been invoked to explain the barrier. In this Letter, we show that correct barriers arise naturally when embedded correlated electron wave functions are used to capture the physics of the interaction of O_2 with the metal surface. The barrier originates from an abrupt charge transfer (from metal to oxygen), which is properly treated within correlated wave function theory but not within conventional density functional theory. Our potential energy surfaces also identify oxygen atom abstraction as the dominant reaction pathway at low incident energies, consistent with measurements, and show that charge transfer occurs in a stepwise fashion.

Understanding the interaction of gas molecules with metal surfaces is critically important for many applications including molecular sensing, catalysis, and corrosion. The initial dissociative sticking of gas molecules such as molecular oxygen (O_2) enables subsequent reactions through catalysis [1,2]. Conversely, surface corrosion engenders considerable costs [3]. Despite their importance, the details of these processes are poorly understood [4]. Even for the simple yet prominent benchmark case of O_2 approaching an ideal aluminum (111) surface [Fig. 1(a)], there is a troubling discrepancy between theory and experiment: experiments consistently suggest the existence of an energy barrier [5–7] preventing low-energy sticking. However, studies [8–10] employing conventional Kohn–Sham density functional theory (KS DFT) show no such barrier. There is an ongoing debate whether the measured energy barrier is due to spin quenching or charge transfer [4]. Furthermore, experiments consistently find widely spaced oxygen atoms instead of pairs (as one would expect from full chemisorption of O_2), especially at low incident energies [6,11]. Various mechanisms to explain these observations have been proposed, including abstraction [6,12], dissociation [13], and hot-atom motion [11,14].

Recent constrained KS DFT calculations related the origin of the energy barrier to spin selection rules [15,16], as suggested by Ref. [7]. By contrast, earlier simulations employing semiempirical potentials proposed nonadiabatic charge transfer from the surface to O_2 [17]. Subsequent calculations of the interaction between O_2 and small Al clusters support the latter model: using correlated wave function methods, they suggest the approximate treatment

of exchange correlation (XC) in KS DFT as reason for its failure [18–20]. Local (or semilocal) density-based XC functionals lack derivative discontinuities [21] and suffer from self-interaction error due to their lack of exact exchange [22]. These two XC flaws within pure DFT produce overdelocalization of electrons. We therefore expect an unphysically facile charge transfer between O_2 and the Al surface with conventional KS DFT [18–20]. To obtain
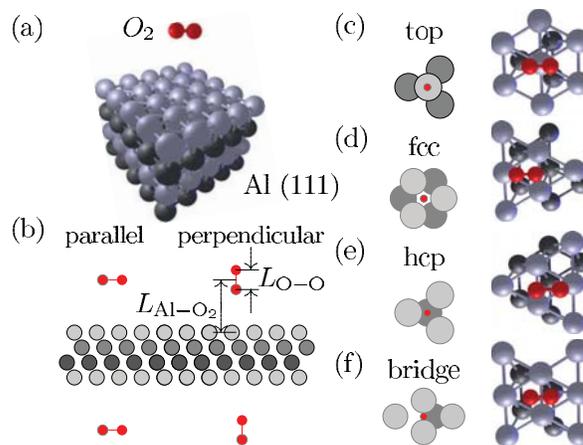

FIG. 1 (color online).   (a) Four-layer Al(111) periodic slab and approaching O_2 molecule. (b) Geometries used in this work to investigate different points of the Al(111) surface. Both perpendicular and parallel incidence of O_2 were investigated. (c–f) The four different high-symmetry positions of the Al(111) surface, and the respective embedded two-layer clusters used in our calculations.

a reliable picture of the charge transfer process, one would need to apply correlated wave function methods to the entire O_2/Al system [Fig. 1(a)], which is too computationally demanding to be feasible. In this Letter, we solve this problem by using a recently developed embedding theory [23] that allows for a completely *ab initio* description of the interaction between O_2 and its nearby Al atoms at the different possible adsorption sites [Figs. 1(c)–1(f)], while the rest of the Al surface is treated by KS DFT. The two subsystems interact via a unique, formally exact embedding potential [23]. We aim for a detailed understanding of the reaction, including possible reaction pathways and their associated energy barriers. Our results provide novel quantitative insights into previous measurements [5,6] and implicate activated charge transfer as fundamental to the O_2/Al adsorption process. The highly accurate *ab initio* potential energy surfaces obtained in this work may also serve as a basis for future dynamics simulations of the reaction of oxygen with aluminum surfaces.

We consider an O_2 molecule approaching an Al(111) surface at different orientations and adsorption sites [Fig. 1]. We map out the ground state energy as a function of the O_2 bond length L_{O-O} and the distance of the molecule's center-of-mass to the Al surface L_{Al-O_2} [see, e.g., Fig. 2(a)]. For a pure KS DFT description, we use an Al slab [Fig. 1(a)] described by a periodic 5×5 supercell (for details see Refs. [24–26]). To elucidate the role of exchange and correlation, we then treat the same problem with highly accurate correlated wave function (CW) methods (second-order multireference many-body perturbation theory [26,27]). We cut a small cluster of 10 to 14 atoms out of the Al slab to model the different possible adsorption

sites [Figs. 1(c)–1(f)]. We then calculate an embedding potential V_{emb} representing the interaction between the cluster and the remaining Al(111) surface [23]. The ground state energy of this embedded cluster in the presence of O_2 is then determined both on a KS DFT (E_{emb}^{DFT}) as well as a CW (E_{emb}^{CW}) level. Comparing these two energies yields a correction accounting for XC effects beyond the pure KS DFT slab calculation E^{DFT}, so that the final embedded energy E_{emb} can be written as [23]

$$E_{emb} = E^{DFT} + E_{emb}^{CW} - E_{emb}^{DFT}. \qquad (1)$$

Several software packages [24,27–32] were used to evaluate Eq. (1). For technical details, we refer the interested reader to Ref. [23] and the supplemental material Ref. [26].

As discussed in the introduction, conventional KS DFT calculations with local (or semilocal) density-based XC functionals cannot correctly describe the charge transfer process involved in chemisorption of O_2 on Al(111). Accordingly, we find no energy barrier in our KS DFT slab calculations [Fig. 2(a)], and an unphysically smooth transfer of charge from the metal surface to the O_2 molecule (not shown). Our results change qualitatively upon considering our embedded CW energy [Eq. (1)]: the resulting embedding-based potential energy surfaces (EPESs) feature pronounced energy barriers for all surface sites we consider [Figs. 2(b) and 2(c) and Table I]. The maximum cluster-size-converged barrier height (660 meV, Table I) appears consistent with experiments measuring the initial sticking probability of O_2 on Al(111) as function of O_2 kinetic energy. Almost no increase of sticking probability is observed at energies above 600 meV [5]. Fluctuations in the CW results due to inaccuracies of the perturbative
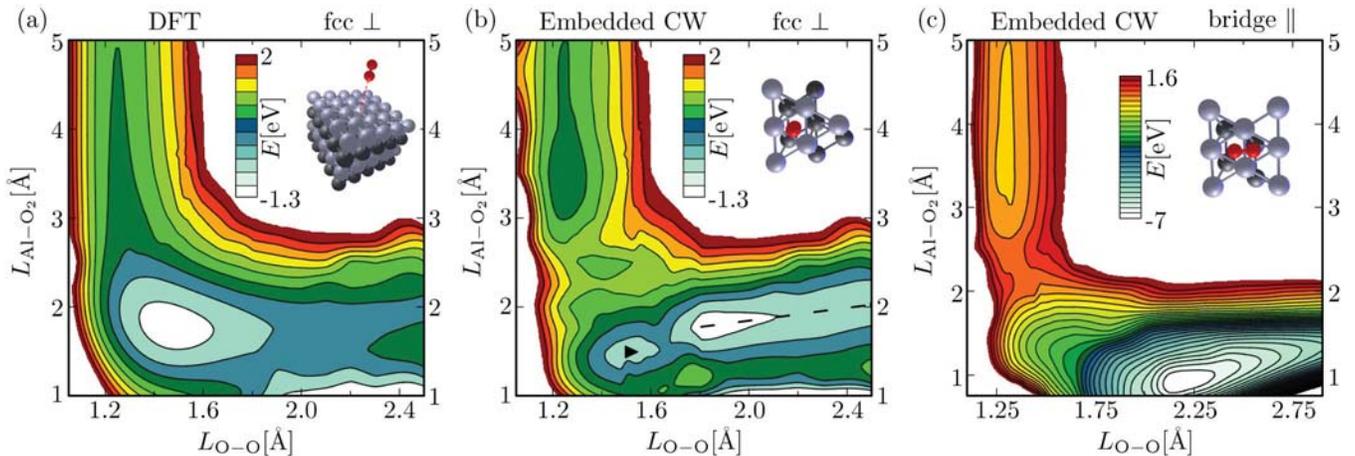

FIG. 2 (color online). (a) PES calculated using KS DFT with a periodic slab model for O_2 approaching perpendicular to the fcc hollow site on the Al(111) surface [see inset and Fig. 1]. (b) Same O_2 site and orientation as (a), now based on embedded correlated wave functions [Eq. (1), 6/6 cluster geometry, see inset]. Barrier height is 360 meV (Table I). Black triangle marks an intermediate local minimum and dashed line an elongated minimum within a reaction pathway towards O_2 abstraction. (c) Same method as (b) for the Al(111) bridge site with O_2 parallel to the surface (8/4 cluster geometry, see inset). Barrier height is 530 meV (see Table I and Fig. 1 in Ref. [26]). Increasing cluster size to 8/6 increases the barrier height by only 30 meV (see Table I). Minimum of the embedding-based PES at $L_{Al-O_2} = 0.9$Å and $L_{O-O} = 2.2$ Å. Energy spacing between contour lines is 300 meV.

TABLE I. Embedded CW predictions of the barrier height and surface distance at the top of the barrier for different adsorption sites (Fig. 1), cluster sizes, and O_2 orientations. Errors represent fluctuations in the final EPES.

Site	No. of atoms		Orientation	$E^{barrier} \pm \delta$ (meV)	$L^{barrier}_{Al-O_2}$ (Å)
	1st layer	2nd layer			
bridge	8	6	$\parallel$	560 ± 10	2.4
	8	6	$\perp$	450 ± 30	2.7
fcc	6	6	$\parallel$	430 ± 20	2.4
	6	6	$\perp$	360 ± 10	2.9
hcp	6	6	$\parallel$	410 ± 10	2.5
	6	6	$\perp$	410 ± 20	2.9
top	7	3	$\parallel$	660 ± 20	2.6
	7	3	$\perp$	660 ± 20	2.8
experiment [5]				$\lesssim 600$	

expansion are below 30 meV (Table I). We note that too-small clusters (with less than ten atoms) overestimate the energy barrier for the charge transfer [26], due to the smaller amount of polarizable screening (V_{emb} is not self-consistently updated during charge transfer). Calculations of clusters larger than 14 atoms quickly become unfeasible due to the computational demands of the complete active space self-consistent field method [26]. We also calculate energy barriers for several different cluster geometries at the same adsorption site and find variations $\lesssim 60$ meV [26]. We thus estimate a final uncertainty of ≈ 100 meV in the barrier heights caused by the finite cluster size and the nonself-consistent V_{emb} [26].

To investigate the origin of the energy barrier, we calculate the charge and spin states of the oxygen molecule as it approaches the surface. We find an abrupt charge transfer, accompanied by a change of O_2 spin, at the barrier [Fig. 3]; i.e., the corresponding diabatic surfaces cross. Far from the Al surface, the triplet state is energetically favored. At $L_{Al-O_2} \approx 2.5$ Å [Table I], a first charge transfer occurs to form O_2^- and a doublet spin configuration at the O_2 becomes preferred [Fig. 3]. The transfer starts at larger L_{Al-O_2} for larger L_{O-O}, consistent with the increased sticking probability of vibrationally excited O_2 found in experiment [5].

To assess the importance of including an embedding potential, we compare (see Table 1 in Supplemental Material Ref. [26]) the EPES with data obtained from an isolated, nonembedded Al cluster treated at the CW level. While abrupt charge transfer at the crossing of the barrier is still predicted, the relative barrier heights are incorrect: the barrier for abstraction is much higher than for dissociative adsorption, which is not consistent with (and is in fact the reverse of) experiment. The embedding potential provides the correct boundary condition at the edges of the cluster needed to obtain the correct electronic structure inside the Al cluster. The correct boundary condition is key to obtaining correct trends and quantitative results.

After crossing the barrier, one or both of the oxygen atoms may adsorb. To investigate possible reaction pathways, we calculate the energy E_O [using Eq. (1)] of a single oxygen atom at various surface positions. We find two minima at the fcc (hcp) positions, separated by 1.6 Å and with energies of 8.3 eV (8.1 eV) lower than the energy of an oxygen atom at 5 Å above the surface. For O_2 parallel incidence upon the bridge site, both oxygen atoms will be aligned with these minima. Indeed, the corresponding EPES for O_2 dissociation features an associated minimum, albeit with a smaller $E_{emb} = -6.8$ eV at a larger $L_{O-O} = 2.2$ Å [Fig. 2(c)], due to Coulomb repulsion between the two charged oxygen atoms [26].

The above energy considerations allow for a second possible reaction pathway: the energy gain of 8.3 eV upon adsorption of one O atom is large enough to permit dissociative adsorption of one atom while the second atom is emitted into the gas phase as a free radical, a process commonly referred to as abstraction. Let us consider the fcc site and perpendicular incidence, as the closer oxygen atom will be in a favorable adsorption position. The corresponding EPES indeed suggests abstraction for
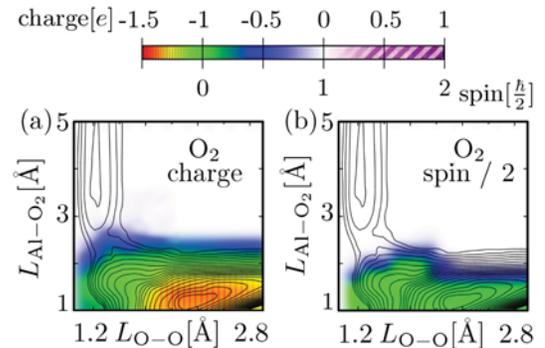

FIG. 3 (color online). (a) Mulliken charge populations and (b) Mulliken spin populations for O_2 approaching the bridge site in parallel incidence. The contour lines of the potential energy surface [Fig. 2(c)] are superposed to guide the eye.

perpendicular incidence: we observe a minimum extending up to $L_{O-O} = 2.5$ Å [see dashed line in Fig. 2(b)] that is not present for KS DFT [Fig. 2(a)]. The relative barrier heights of perpendicular and parallel incidence for the embedded CW calculations [Table I] suggest abstraction is likely to be a dominant pathway at low energies, consistent with the observation of a large fraction of single oxygen atoms on the metal surface in STM measurements at low incident energies [6]. As in the parallel case, we find abrupt transfer of charge and change of spin [Fig. 4]. However, now there is a strong asymmetry between charges on the two O atoms: only small amounts of charge are transferred to the farther oxygen [Fig. 4(b)] that returns to a triplet configuration at $L_{O-O} > 1.6$ Å [Fig. 4(d)], in line with the ^3P ground state of an isolated oxygen atom, leaving the adsorbed oxygen and the cluster in a spin-free singlet state. Conversely, the closer oxygen takes nearly the same charge as the entire O_2 molecule in the parallel case [compare Figs. 3(a) and 4(a)]. Thus, the EPES suggests that abstraction happens in a three-step process: (i) crossing the initial barrier, 0.5 e charge transfers to the closer atom; (ii) another 0.5 e transfers to form O_2^- in a shallow local minimum [17] of the potential energy surface [see triangle in Fig. 4]; and finally, (iii) dissociation of a neutral O in its ^3P ground state, while the remaining O bonds with the Al surface as a negatively charged adsorbate.

Finally, we compare our results to previous theoretical models, in particular nonadiabatic [17] or diabatic [16] approaches, which also find an energy barrier consistent with experiment. However, unlike the earlier reports, our description contains no adjustable model parameters or specially designed XC functionals; the barriers arise

FIG. 4 (color online). Mulliken charge [(a–b)] and spin [(c–d)] populations for close and far O atoms in O_2 in perpendicular incidence above the fcc site [Fig. 2(b), contour lines of the EPES with a line spacing of 400 meV are plotted in black to guide the eye]. Black triangles mark an intermediate local minimum along a reaction pathway towards O_2 abstraction. Colors refer to legend given in Fig. 3.

naturally when electron exchange and correlation are properly accounted for. Secondly, our relative barrier heights are consistent both with the experimental observation of singly absorbed oxygen atoms at low incident kinetic energies and the observed maximum energy threshold for sticking. By contrast, spin-restricted calculations overestimate the barrier height for abstraction because the metastable intermediate related to O_2^- [see triangle in Fig. 4(a)] is absent [15]. To investigate whether the spin selection rules proposed by Ref. [16] are necessary to account for the barrier, we additionally calculated the singlet EPES. We find minimal differences between the triplet and singlet EPESs, which indicates a very small energy (≈ 50 meV) required to change the spin of the embedded metal cluster, and hence, of the entire system. Put differently, the metal surface easily adopts, within reasonable limits, an arbitrary spin configuration, thus, substantially decreasing the energy difference between different $\langle \hat{S}^2 \rangle$ quantum numbers for the entire system. Indeed, at room temperature, $\langle \hat{S}^2 \rangle$ of an infinitely extended Al surface changes under the influence of thermal fluctuations. Lastly, we note that although DFT fails to describe dissociative adsorption of O_2 on Al(111), similar calculations for seemingly more complex transition metals like palladium or platinum are modeled reasonably well [33]. We attribute this discrepancy to the small work function of Al(111), 4.26 eV, combined with the delocalized nature of its valence electrons, which greatly facilitates charge transfer and, coupled with DFT XC errors, leads to no barrier within DFT. The higher work functions for Pt(111) of 5.93 eV and Pd(111) of 5.6 eV [34] result in an energy cost for charge transfer which can even be seen within DFT.

In conclusion, we investigated the interaction of O_2 with Al(111) using highly accurate embedded correlated wave function methods [23]. Unlike conventional KS DFT calculations, our results agree with experimental observations, showing finite energy barriers at all high-symmetry points of the surface, for both parallel and perpendicular orientations of O_2. The barrier arises from the energetic cost to initiate abrupt charge transfer from the metal surface to the molecule; the self-interaction error and the lack of the derivative discontinuity in approximate DFT XC cause spuriously easy charge transfer with no barrier predicted. By correctly evaluating charge transfer with a correlated wave function theory, we show there is no need to invoke nonadiabatic surface hopping or spin selection rules to explain the barrier. In reality, abrupt spin changes at the crossings of different diabatic O_2 spin configuration surfaces are accommodated by small spin fluctuations within the metal surface. For parallel incidence, the potential energy surface points to direct adsorption at two adjacent fcc-hcp hollow sites of the Al(111) surface. By contrast, we predict abstraction at perpendicular incidence: our results not only support this mechanism as dominant pathway at low incident energies (as proposed by STM investigations),
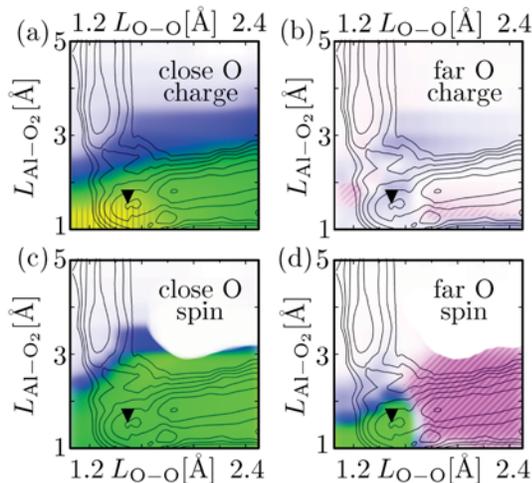
but also provide exquisite detail of charge and spin changes along the pathway. Of course, conclusions drawn strictly from PESs may miss dynamical details such as steering events. Future quantum dynamics simulations based on our EPES may confirm the proposed mechanism.

---

*Permanent address: Department of Chemistry, University of Napoli Federico II, Napoli 80120, Italy

†eac@princeton.edu

[1] T. Zambelli, J. V. Barth, J. Wintterlin, and G. Ertl, Nature (London) **390,** 495 (1997).

[2] P. A. Kilty and W. M. H. Sachtler, Catal. Rev. **10,** 1 (1974).

[3] M. Ryan, Nature Mater. **3,** 663 (2004).

[4] J. J. Kroes, Science **321,** 794 (2008).

[5] L. Österlund, I. Zorić, and B. Kasemo, Phys. Rev. B **55,** 15452 (1997).

[6] A. J. Komrowski, J. Z. Sexton, A. C. Kummel, M. Binetti, O. Weiße, and E. Hasselbrink, Phys. Rev. Lett. **87,** 246103 (2001).

[7] M. Binetti and E. Hasselbrink, J. Phys. Chem. B **108,** 14 677 (2004).

[8] T. Sasaki and T. Ohno, Surf. Sci. **433-435,** 172 (1999).

[9] K. Honkala and K. Laasonen, Phys. Rev. Lett. **84,** 705 (2000).

[10] Y. Yourdshahyan, B. Razaznejad, and B. I. Lundqvist, Phys. Rev. B **65,** 075416 (2002).

[11] H. Brune, J. Wintterlin, R. J. Behm, and G. Ertl, Phys. Rev. Lett. **68,** 624 (1992).

[12] M. Binetti, O. Weiße, E. Hasselbrink, A. J. Komrowski, and A. C. Kummel, Faraday Discuss. Chem. Soc. **117,** 313 (2000).

[13] M. Schmid, G. Leonardelli, R. Tscheließnig, A. Biedermann, and P. Varga, Surf. Sci. **478,** L355 (2001).

[14] H. Brune, J. Wintterlin, J. Trost, G. Ertl, J. Wiechers, and R. J. Behm, J. Chem. Phys. **99,** 2128 (1993).

[15] J. Behler, K. Reuter, and M. Scheffler, Phys. Rev. B **77,** 115421 (2008).

[16] J. Behler, B. Delley, S. Lorenz, K. Reuter, and M. Scheffler, Phys. Rev. Lett. **94,** 036104 (2005).

[17] G. Katz, R. Kosloff, and Y. Zeiri, J. Chem. Phys. **120,** 3931 (2004).

[18] C. Mosch, C. Koukounas, N. Bacalis, A. Metropoulos, A. Gross, and A. Mavridis, J. Phys. Chem. C **112,** 6924 (2008).

[19] N. C. Bacalis, A. Metropoulos, and A. Gross, J. Phys. Chem. A **114,** 11 746 (2010).

[20] E. Livshits, R. Baer, and R. Kosloff, J. Phys. Chem. A **113,** 7521 (2009).

[21] J. P. Perdew, R. G. Parr, M. Levy, and J. L. Balduz, Phys. Rev. Lett. **49,** 1691 (1982).

[22] J. P. Perdew and A. Zunger, Phys. Rev. B **23,** 5048 (1981).

[23] C. Huang, M. Pavone, and E. A. Carter, J. Chem. Phys. **134,** 154110 (2011).

[24] G. Kresse and J. Furthmüller, Comput. Mater. Sci. **6,** 15 (1996).

[25] J. P. Perdew, K. Burke, and M. Ernzerhof, Phys. Rev. Lett. **77,** 3865 (1996).

[26] See Supplemental Material at http://link.aps.org/supplemental/10.1103/PhysRevLett.109.198303 for technical details of the computations and further convergence studies.

[27] K. Andersson, P.-A. Malmqvist, and B. O. Roos, J. Chem. Phys. **96,** 1218 (1992).

[28] X. Gonze *et al.,* Comput. Phys. Commun. **180,** 2582 (2009).

[29] X. Gonze, Z. Kristallogr. **220,** 558 (2005).

[30] F. Aquilante *et al.,* J. Comput. Chem. **31,** 224 (2010).

[31] M. W. Schmidt *et al.,* J. Comput. Chem. **14,** 1347 (1993).

[32] M. Gordon, *Theory and Applications of Computational Chemistry: the First 40 Years* (Elsevier, Amsterdam, 2005), p. 1167.

[33] A. Eichler and J. Hafner, Phys. Rev. Lett. **79,** 4481 (1997); A. Eichler, F. Mittendorfer, and J. Hafner, Phys. Rev. B **62,** 4744 (2000).

[34] *CRC Handbook of Chemistry and Physics,* edited by W. M. Haynes and D. R. Lide (CRC Press, Boca Raton, 2011), 92nd ed.